Workfunction-Tunable, N-Doped Reduced Graphene Transparent Electrodes for High-Performance Polymer Light-Emitting Diodes

Jin Ok Hwang,[†,∥] Ji Sun Park,[†,∥] Dong Sung Choi,[†] Ju Young Kim,[†] Sun Hwa Lee,[†] Kyung Eun Lee,[†] Yong-Hyun Kim,[‡] Myoung Hoon Song,[§] Seunghyup Yoo,[⊥] and Sang Ouk Kim[†,*]

[†]Department of Materials Science and Engineering, KI for the Nanocentury, KAIST, Daejeon, 305-701, Republic of Korea, [‡]Graduate School of Nanoscience and Technology (WCU), KAIST, Daejeon, 305-701, Republic of Korea, [§]School of Mechanical and Advanced Materials Engineering, Ulsan National Institute of Science and Technology (UNIST), Banyeon-ri 100, Ulsan 689-805, Republic of Korea, and [⊥]Department of Electrical Engineering, KAIST, Daejeon, 305-701, Republic of Korea. [∥]These authors equally contributed to this work.

ABSTRACT

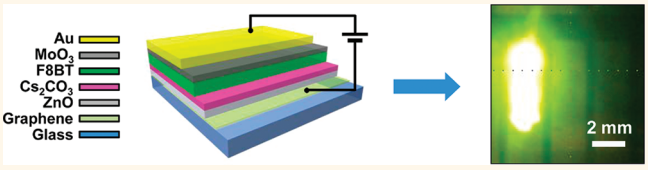

Graphene is a promising candidate to complement brittle and expensive transparent conducting oxides. Nevertheless, previous research efforts have paid little attention to reduced graphene, which can be of great benefit due to low-cost solution processing without substrate transfer. Here we demonstrate workfunction-tunable, highly conductive, N-doped reduced graphene film, which is obtainable from the spin-casting of graphene oxide dispersion and can be successfully employed as a transparent cathode for high-performance polymer light-emitting diodes (PLEDs) as an alternative to fluorine-doped tin oxide (FTO). The sheet resistance of N-doped reduced graphene attained 300 Ω/□ at 80% transmittance, one of the lowest values ever reported from the reduction of graphene oxide films. The optimal doping of quaternary nitrogen and the effective removal of oxygen functionalities *via* sequential hydrazine treatment and thermal reduction accomplished the low resistance. The PLEDs employing N-doped reduced graphene cathodes exhibited a maximum electroluminescence efficiency higher than those of FTO-based devices (4.0 cd/A for FTO and 7.0 cd/A for N-doped graphene at 17 000 cd/m^2). The reduced barrier for electron injection from a workfunction-tunable, N-doped reduced graphene cathode offered this remarkable device performance.

KEYWORDS: doping · graphene · workfunction · electrode · light-emitting diode

The unanticipated exfoliation of graphene by micromechanical drawing triggered tremendous research interest in graphene and graphene-based materials.[1,2] The idealized atomic scale structure of graphene composed of monolayered conjugated graphitic carbons presents numerous extraordinary material properties, including high electrical/thermal conductivity,[1,3] flexible but strong mechanical properties,[4,5] high thermal/chemical stability,[6−8] and extremely large surface area,[9] within a genuine two-dimension material. Such an unprecedented synergistic combination of versatile properties renders graphene and graphene-based materials promising components for carbon-based functional materials and devices.[10−20]

The optoelectronic application of graphene has been motivated from the optical transparency,[5,17,18,21] mechanical flexibility, and high electroconductivity of graphene, which potentially complement or are alternatives for high-cost, mechanically brittle transparent conductive oxides (TCOs). Currently, the chemical vapor deposition (CVD) growth of graphene has been considered the most promising preparation method that can address the challenging requirements for transparent electrodes, such as large-area growth and high electroconductivity.[5,22] Nevertheless, the expensive high-temperature batch production and technological challenges for substrate transfer without contamination, wrinkling, and damage of graphene pose formidable technological challenges.[23,24] As an alternative, chemically derived reduced graphene obtainable from natural graphite *via* oxidative exfoliation and subsequent reduction has been suggested as an effective counterplan to exploit a low-cost solution processing without substrate transfer.[25−34] However, currently available postreduction methods to restore the structure and properties of graphene give rise to the incomplete recovery of graphitic structure

* Address correspondence to sangouk.kim@kaist.ac.kr.

Received for review August 18, 2011 and accepted November 11, 2011.

Published online December 13, 2011
10.1021/nn203176u

with many defects and electron-trapping oxygen functional groups, resulting in significantly deteriorated electroconductivity and other material properties.

In this work, we demonstrate an optimized reduction and substitutional N-doping of spin-cast graphene oxide film and its successful application to transparent cathodes for high-performance inverted polymer light-emitting diodes (iPLEDs). An ultrathin graphene oxide film was spin-cast from an aqueous dispersion onto a display-grade glass substrate and was chemically and thermally reduced and N-doped. Owing to the effective reduction accompanied by highly stable substitutional doping of electron-rich N, the resultant reduced graphene film attained a sheet resistance of ~300 Ω/□ at 80% optical transparency, which is one of the lowest values ever reported for reduced graphene film prepared from graphene oxide.[35−39] Moreover, the work-function of the graphene electrodes could be precisely tuned by the N-doping level, and also a low work-function N-doped reduced graphene film[40] has been successfully employed as transparent cathodes of iPLEDs.[41−51] A reduced electron injection barrier from the N-doped graphene cathode in iPLEDs accomplished remarkable device performance comparable to that of the device employing commercially available FTO electrodes.

RESULTS AND DISCUSSION

The preparation of an N-doped reduced graphene electrode and the fabrication of iPLEDs are schematically described in Figures 1a−c. An aqueous dispersion of graphene oxide (concentration: 3.1 mg/mL) was prepared by a modified Hummers method and purified by dialysis. The effective removal of ionic and acidic impurities by dialysis enabled a highly concentrated (more than 5 wt %) dispersion of monolayer-dominant (>95%) graphene oxide sheets.[14] The graphene oxide aqueous solution was spin-cast onto display-grade glass substrates (Corning 1737). This commercially available glass substrate widely used in liquid crystal display devices is thermally stable up to 750 °C, allowing a high-temperature reduction and doping of graphene oxide film. The graphene oxide films on glass substrates were systematically reduced and N-doped by one of three different strategies: (i) chemical treatment with hydrazine vapor, (ii) thermal treatment at 750 °C under a H_2/NH_3 gas mixture, or (iii) sequential chemical and thermal treatments. The straightforward solution casting onto a transparent glass substrate followed by chemical and thermal reductions and doping ensured a scalable arbitrary large-area casting of a transparent conductive film, while avoiding the technological challenges caused by substrate transfer. Furthermore, unlike CVD graphene, a ripple-free uniform film with a surface rms (root-mean-square) roughness of ~0.58 nm was attainable (Supporting Information Figure S1). This high surface uniformity was crucial for the further multilayer device fabrication involved with spin-casting or other solution processing.

The iPLEDs with a green-light-emitting polymer, poly(9,9′-dioctylfluorene)-*co*-benzothiadiazole (F8BT), were fabricated by employing N-doped reduced graphene films on glass substrates as transparent cathodes (Figure 1c). For a minimized oxygen contamination, the devices were fabricated in a glovebox or a vacuum chamber immediately after the preparation of reduced graphene electrodes. Unlike conventional PLED architectures consisting of transparent anodes and low-workfunction metallic cathodes,[52,53] this inverted architecture employed reduced graphene film as a transparent cathode and a high-workfunction metal (Au) as an anode, respectively. Consequently, this architecture was free from oxidative degradation of low-workfunction metal (Ca or Ba) cathodes, which frequently causes poor environmental stability and limited lifetime in conventional PLEDs.[54,55] The ZnO layer and MoO_3 layer were employed as electron and hole transport layers, respectively. The Cs_2CO_3 layer acted as a hole-blocking layer to minimize the hole leakage at the cathode and thereby maximize the electron−hole recombination. We note that this iPLED architecture usually demonstrates hole-dominant device characteristics owing to the unprecedented barrier-free hole injection mediated by the MoO_3 hole transport layer.[43] Therefore, the enhancement of electron injection at the cathode is a crucial requirement for optimized and balanced device operation.

Figure 1d shows the UV−vis spectrum of a typical reduced graphene film used in this work. Owing to the highly dispersed monolayer graphene oxide dispersion, the thickness and corresponding optical transmittance of a graphene film could be precisely controlled by the spinning rate and concentration of graphene oxide dispersion. In this work, the graphene film thickness was fixed at ~4 nm with an optical transparency of 80% at 550 nm (Supporting Information Figure S1). This value is acceptable for usual transparent electrode applications. Since monolayer graphene absorbs ~2.3% of visible light,[21] the 80% transparency indicates eight- or nine-layer stacking (reduced graphene generally has a thickness of ~5 Å, slightly larger than 3.5 Å of native graphene). After film casting, optimized reduction and N-doping conditions were explored to minimize the sheet resistance of a graphene film. In general, doping intentionally introduces impurities for the purpose of modifying electrical properties. A doped semiconductor acts more like a conductor than a semiconductor due to the enhanced electron or hole density supplied from the dopant. In this work, N with a similar atom size but one more valence electron than C was used as the atomic dopant to enhance the electron density in the graphitic plane. Nitrogen was supplied from hydrazine (N_2H_4) and ammonia (NH_3) during chemical and thermal reductions, respectively. First, spin-cast graphene oxide films were divided into two groups. One group was chemically

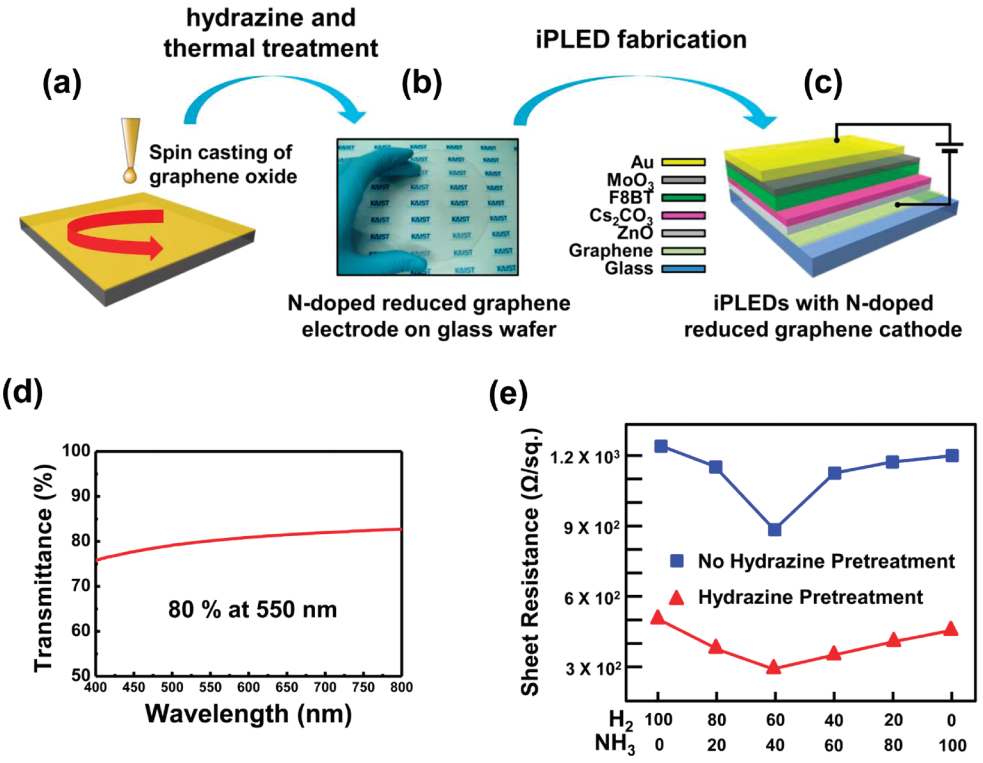

Figure 1. (a–c) Schematic description of preparation and optoelectronic transparent electrode utilization of N-doped reduced graphene film. (d) UV–vis spectrum of the N-doped graphene film. (e) Sheet resistances of hydrazine-untreated and -pretreated reduced graphene films as a function of the H_2/NH_3 ratio during thermal reduction.

treated with hydrazine vapor for 1 h in a sealed vessel, whereas the other group was maintained without any treatment. The two groups were subsequently thermal-treated at 750 °C for 5 min under various flow ratios of H_2/NH_3 mixed gas.

Figure 1e shows the variation of the sheet resistance (R_s) of reduced graphene film as a function of the H_2/NH_3 ratio during thermal treatment (Supporting Information Table S1). The R_s values of both hydrazine-treated and untreated samples showed "V" shapes with the minima at the 6:4 H_2/NH_3 ratio, which demonstrates that appropriate N content during thermal treatment was crucial to achieve a high conductivity. More significantly, the R_s values of hydrazine-pretreated samples were lower than those of untreated samples over the entire H_2/NH_3 ratio. The lowest sheet resistance value of 300 Ω/□ was obtained for the thermal treatment of hydrazine-pretreated graphene oxide film under a gas flow rate of 60 sccm H_2/40 sccm NH_3. To confirm the N-doping effect,[35,36] Hall measurement based on the van der Pauw method was performed for the reduced graphene film with the lowest sheet resistance of 300 Ω/□. As anticipated, the major carrier type was the electrons due to the N-doping. The measured sheet carrier density (1.98×10^{15} cm^{-2}) was consistent with the value calculated from the measured sheet resistance (Hall measurement in Supporting Information).

The amounts of N dopant and remaining O in the reduced graphene films were characterized by X-ray photoelectron spectroscopy (XPS). Figure 2a and b represent the narrow scan spectra for the N and O range of untreated and hydrazine-treated samples, respectively. The N and O contents of untreated samples varied over a broad range with the H_2/NH_3 ratio. In contrast, those of the hydrazine-pretreated samples showed a less pronounced variation. In particular, N contents were maintained with almost the same values of ~2.6% over the entire H_2/NH_3 ratio (Figure 2b and d). We note that the O content of graphene oxide was 28.0%, and the N and O contents of hydrazine-treated graphene oxide were 7.3% and 12.5%, respectively, before thermal treatment (Supporting Information Figure S2). It is evident that hydrazine treatment greatly lowered the O content of graphene oxide and further thermal treatment removed less stable N and O atoms presumably present at physisorbed molecules or dangling bonds. We note that the overall "V" shape variation of R_s shown in Figure 1e is closely related to the variation of the O/C ratio shown in Figure 2c. Effective O removal by sequential chemical and thermal reductions was crucial to achieve a high conductivity of reduced graphene oxide films.

As previously reported, N-doping can enhance the electron density and thereby lower the workfunction of graphitic carbon materials.[56–58] The workfunction of N-doped reduced graphene film was measured by ultraviolet photoelectron spectroscopy (UPS) (Supporting Information Table S1). The measured workfunction was

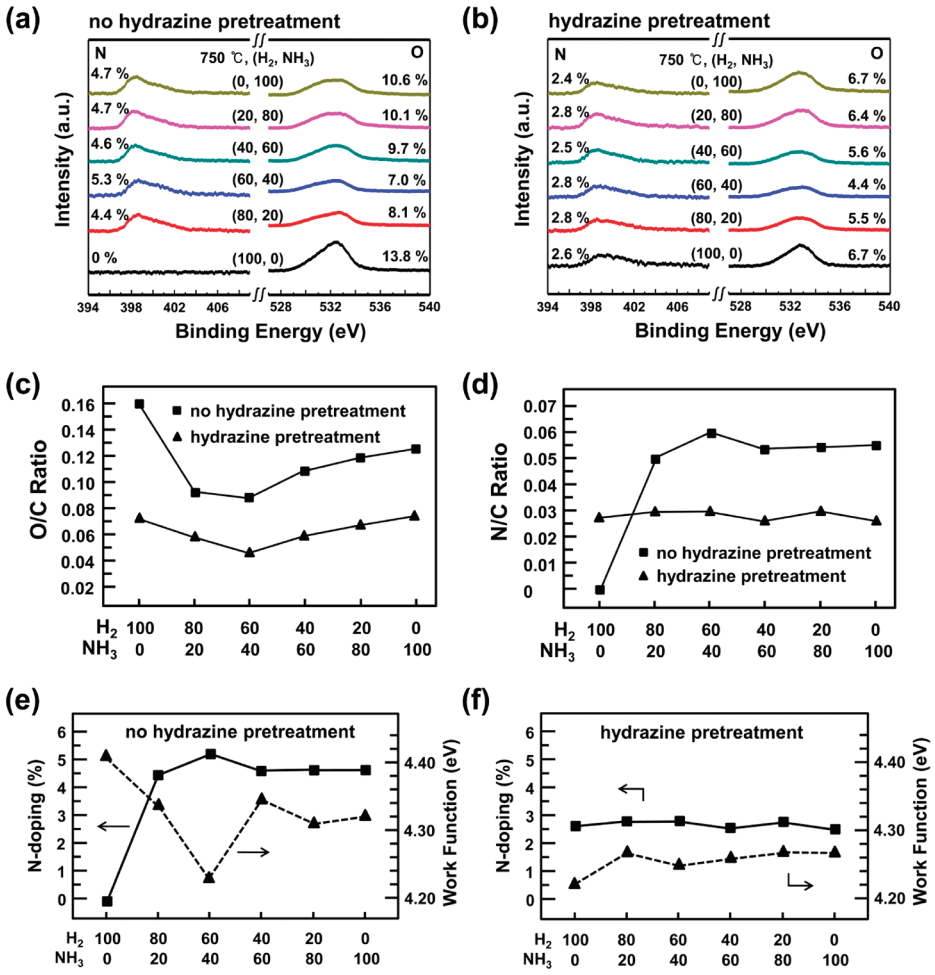

Figure 2. XPS spectra for N and O binding energy range of (a) untreated and (b) hydrazine-pretreated reduced graphene films prepared by various flow ratios of H_2/NH_3 mixed gas at 750 °C. (c) O/C ratio and (d) N/C ratio in reduced graphene films plotted as a function of the H_2/NH_3 ratio during thermal reduction. N-doping levels and workfunctions of (e) untreated and (f) hydrazine-pretreated reduced graphene electrodes.

reciprocally proportional to the N-doping level (Figure 2e and f). Films not treated with hydrazine revealed a variation of 4.2−4.4 eV, while hydrazine-pretreated film maintained almost the same value of ~4.25 eV. Compared with the relatively large workfunction of pure graphene (~4.6 eV),[59,60] N-doped reduced graphene revealed significantly lowered workfunction.

Figure 3a shows the high-resolution N1s XPS analysis of bonding configurations of N atoms in reduced graphene films. Each N1s peak could be deconvoluted into three peaks: the lowest energy peak at 398.8−399.1 eV corresponds to pyridinic N (N_{pyri}), the middle energy peak at 400.5−400.7 eV corresponds to quaternary N (N_{qua}), and the highest energy peak corresponds to nitrogen oxide (N_{ox}), respectively.[38,56,65] Among the three observed N-doping types, only N_{qua} is known to improve the electroconductivity of graphene films.[40] N_{pyri} with a localized lone pair of electrons (Figure 3a, upper right) inevitably accompanies a vacancy defect and cannot contribute to the recovery of the graphitic structure. N_{ox} is usually present at N-containing dangling bonds or physisorbed species that cannot contribute to the recovery of hexagonal graphitic structure. In contrast, N_{qua}, a secure substitution of C with N (Figure 3a, upper left), is known to maintain an sp^2-hybridized graphitic structure as well as to improve the electroconductivity by providing delocalized electrons.[56,60−62]

Figure 3b and c demonstrate the ratio of N_{qua} or N_{pyri} normalized by the total amount of N doping (N_{total}) plotted against the H_2/NH_3 ratio. The hydrazine-pretreated sample showed the highest N_{qua}/N_{total} value of ~0.7 at a 6:4 H_2/NH_3 ratio, while the N_{pyri}/N_{total} value was maintained at ~0.3 over the entire H_2/NH_3 ratio. This inverse "V"-shaped plot of the N_{qua}/N_{total} ratio with a maximum at the 6:4 H_2/NH_3 ratio is reciprocally related to the variation of sheet resistance in Figure 1e. It is noteworthy that before thermal treatment the hydrazine-treated graphene oxide showed a much lower N_{qua}/N_{total} value of 0.25 (N_{pyri}/N_{total} values of 0.56) (Supporting Information Figure S2), implying that the high-temperature treatment at 750 °C remarkably improved the N_{qua}/N_{total}. In contrast, the sample not treated with hydrazine revealed N_{qua}/N_{total} values lower than

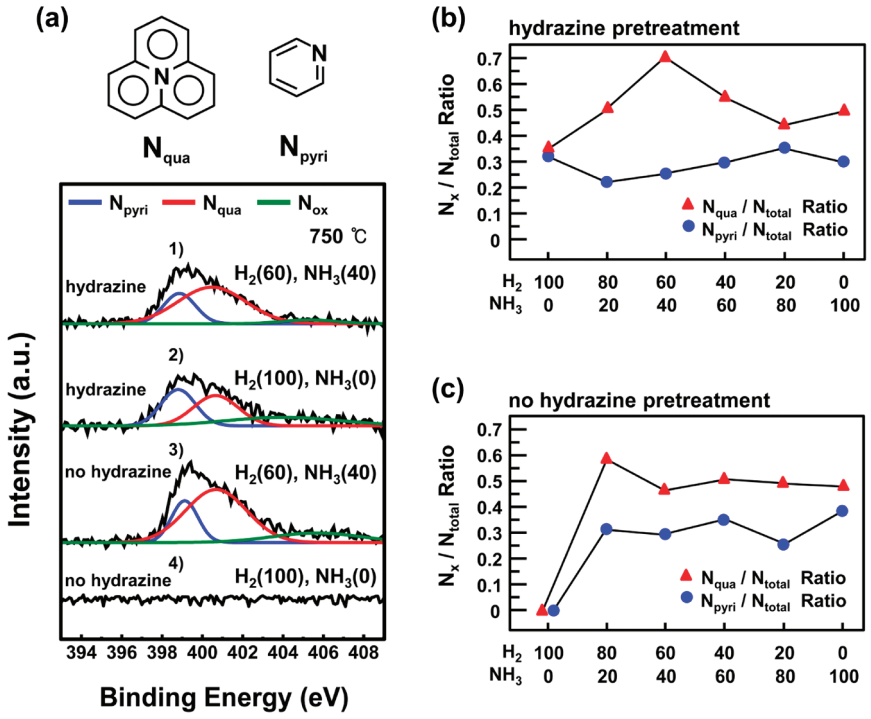

Figure 3. (a) N1s XPS spectra of various reduced graphene films. The N1s peak is deconvoluted into N_{pyri}, N_{qua}, and N_{ox} peaks. The N_{qua}/N_{tot} and N_{pyri}/N_{tot} ratios of (b) hydrazine-pretreated and (c) untreated reduced graphene films as a function of the H_2/NH_3 ratio.

0.6 even after thermal treatment, while the N_{pyri}/N_{total} value stayed at the same level with hydrazine-pretreated samples. Taken together, the highest conductivity of N-doped reduced graphene film with the maximized N_{qua} doping and a minimum amount of remaining O was achieved by the sequential employment of hydrazine treatment and thermal treatment under NH_3 environment.[40]

As summarized in Figure 4a, N-doped reduced graphene films prepared by sequential hydrazine and thermal treatment and simply reduced film prepared by thermal treatment without a nitrogen source have been employed as a cathode of iPLEDs, instead of FTO, a widely used commercially available TCO electrode.[63] We note that the N-doped reduced graphene had a relatively low workfunction (~4.25 eV) compared to other conventional transparent electrodes (4.5−5.2 eV)[64] (Supporting Information Figure S3). Such a low workfunction offered a valuable transparent cathode for inverted-type optoelectronic devices with a minimized electron injection barrier (Figure 4b). Figure 4c shows the luminance (L) as a function of applied voltages (V). We note that the luminance of iPLEDs with N-doped graphene cathodes was quite comparable to the device with conventional FTO electrode for $J < 40$ mA/cm^2, featuring a turn-on voltage even lower than that of the FTO (the turn-on voltage defined at the luminance of 1 cd/m^2 was 5.2 V for FTO and 4.8 V for N-doped graphene, respectively). The inset image of Figure 4c shows the uniform emission of an iPLED employing the N-doped graphene cathodes. Meanwhile, in the relatively high current range ($J > 40$ mA/cm^2), the device with N-doped graphene cathodes suffered from a voltage shift, which was caused by a voltage drop that occurred where the sheet resistance of the transparent cathode became more significant as the current level increases (Supporting Information Figure S4). In contrast, devices with thermally reduced graphene cathodes without N-doping showed a significantly larger turn-on voltage of 8.2 V and lower luminance than other devices (Table 1 for a summary of device characteristics). This shift in the turn-on and operational voltage resulted from the large sheet resistance and significant injection barrier of the reduced graphene caused by the mismatch in energy level with ZnO electron transport layer (Figure 4b).

Figure 4d presents the electroluminescence (EL) efficiency (η_{EL}) plotted against L. The maximum EL efficiency of the device with N-doped graphene was as large as 7.0 cd/A (at ~17 000 cd/m^2), while it was only 4.0 cd/A for FTO-based devices under the same luminance condition (Supporting Information Figure S5 to compare the device efficiencies plotted as η_{EL} *vs* J and η_{EL} *vs* V, respectively). The enhanced luminous efficiency (cd/A) was attributed to the lowered injection barrier of the low workfunction of N-doped graphene cathodes. This is also supported by the $J-V$ characteristics of the electron-only devices, where N-doped graphene cathodes revealed remarkably high electron injection and conduction (Supporting Information Figure S6). The low

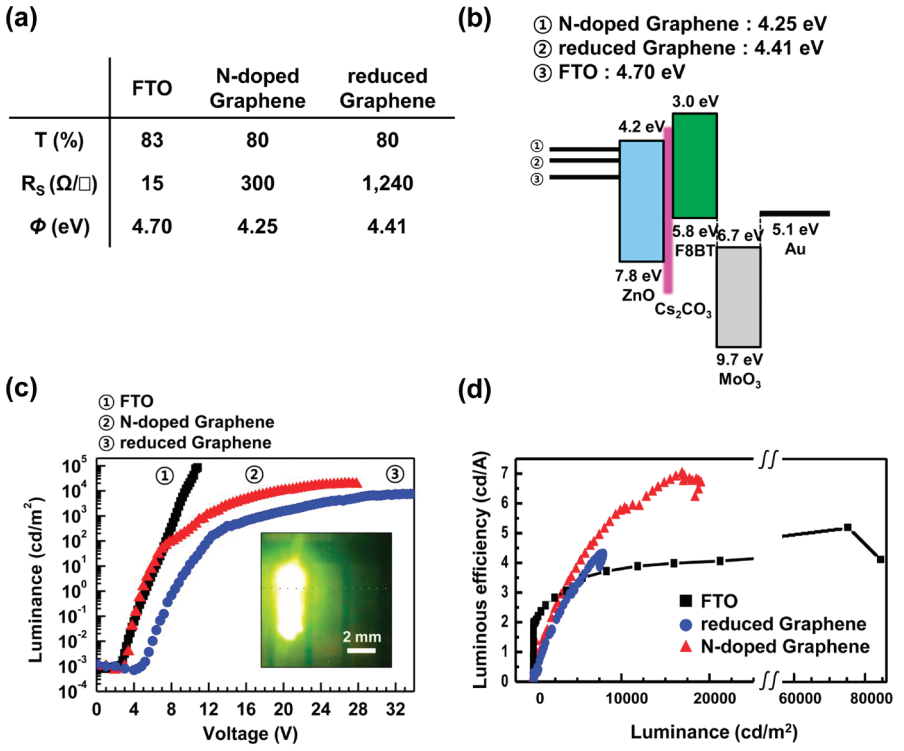

	FTO	N-doped Graphene	reduced Graphene
T (%)	83	80	80
R_S (Ω/□)	15	300	1,240
Φ (eV)	4.70	4.25	4.41

Figure 4. (a) Optical transparency, sheet resistance, and workfunction of FTO, N-doped graphene, and reduced graphene electrodes used for iPLEDs. (b) Energy level diagram of iPLEDs. (c) Luminance *vs* voltage ($L-V$) characteristics of iPLEDs. Inset shows an emission image of iPLEDs with N-doped graphene cathode. (d) Luminous efficiency *vs* luminance ($\eta_{EL}-L$) curves of iPLEDs.

TABLE 1. Light-Emitting Characteristics of iPLEDs Employing FTO, Reduced Graphene, and N-Doped Reduced Graphene Transparent Cathodes

device configuration	max. luminance (cd/m^2) (@ bias)	max. luminous efficiency (cd/A) (@ bias)	max. power efficiency (lm/W) (@ bias)	turn-on voltage (V)[a]
FTO/ZnO/Cs_2CO_3/F8BT/MoO_3/Au	84 540 (@ 10.8 V)	5.2 (@ 10.6 V)	2.6 (@ 10.6 V)	5.2
reduced Graphene/ZnO/Cs_2CO_3/F8BT/MoO_3/Au	7620 (@ 34.0 V)	4.0 (@ 32.8 V)	0.4 (@ 28.8 V)	8.2
N-graphene/ZnO/Cs_2CO_3/F8BT/MoO_3/Au	19 020 (@ 27.0 V)	7.0 (@ 24.2 V)	0.9 (@ 23.0 V)	4.8

[a] Turn-on voltage is defined at the luminance of 1 cd/m^2.

injection barrier at the N-doped graphene cathode/ZnO interface provides a better electron−hole balance, leading to a higher luminous efficiency. This confirms the potential benefit of an N-doped graphene electrode as a low-workfunction transparent cathode. Along with further improvement of electroconductivity, it can play a more significant and practical role in a variety of optoelectronic applications. Even at the present level, the demonstrated performance can be regarded as sufficient in many applications that can benefit from the mechanical flexibility, stretchability, and affordability of graphene electrodes.

CONCLUSIONS

We have demonstrated the fabrication and optoelectronic transparent electrode utilization of workfunction-tunable N-doped reduced graphene films. The optimized reduction and N-doping condition for graphene oxide films uniformly spin-cast onto a display-grade glass substrate were exploited. Hydrazine chemical treatment and subsequent thermal treatment under an ammonia environment were found to generate low-workfunction (4.25 eV) N-doped graphene films with an optical transparency of 80% and sheet resistance of 300 Ω/□, respectively. The detailed XPS analysis confirmed that among the various N-doping types, quaternary N (N_{qua}), which maintains a graphitic structure, plays a crucial role in activating delocalized electrons along with the effective elimination of oxygen functional groups for the lowest sheet resistance of graphene electrodes. Surprisingly, the utilization of highly reduced N-doped graphene film as a transparent cathode of iPLEDs revealed a device performance comparable to that of FTO-based devices. Despite significantly (20 times) larger electroconductivity, the iPLEDs with an N-doped reduced graphene electrode demonstrated comparable device turn-on voltages (2.6 V for FTO and 3.0 V for N-doped graphene) and even higher EL efficiencies (4.0 cd/A for FTO and 7.0 cd/A for N-doped graphene at 17 000 cd/m^2) than

FTO-based devices. The low electron injection barrier given by the low-workfunction N-doped graphene cathode offered such a remarkable device performance. We anticipate that spin-cast, workfunction-tunable, N-doped graphene films could fulfill the role of transparent electrodes for various optoelectronics requiring subtle tunability of energy levels as well as low-cost, large-area processability.

EXPERIMENTAL SECTION

Preparation of N-Doped Reduced Graphene Film. An aqueous graphene oxide dispersion was prepared from commercially available graphite (Aldrich) by a modified Hummers method. After vacuum filtering with 10-fold-diluted hydrogen chloride (Sigma Aldrich, 37%) several times, graphene oxide was vacuum-dried at room temperature. The dried solid powder was redispersed in deionized water to remove residual ionic or acidic impurities by dialysis (Spectrum Laboratory, Inc., MWCO of membrane: 8000). The dialysis was performed for two weeks, occasionally changing the water in the glass bath. After dialysis, the resultant graphene oxide aqueous solution (3.1 mg/mL) was mixed and diluted with ethanol (Sigma Aldrich, ACS reagent, >99.5%) for facile spin-casting onto glass substrates (Coring 1737). A graphene oxide film was prepared by two instances of spin-casting at a spinning rate of 3000 rpm. A group of graphene oxide films were treated under hydrazine vapor for 1 h in a sealed vessel. Both the untreated and hydrazine-pretreated samples were thermally reduced and N-doped with a H_2/NH_3 gas mixture at 750 °C for 5 min.

Fabrication of iPLED Devices. A 70 nm thick ZnO electron transport layer was deposited onto the cleaned FTO, reduced graphene, and N-doped graphene substrate by electron beam evaporation. The Cs_2CO_3 layer was spin-cast onto the ZnO layer from a 0.5 wt % 2-methoxyethanol solution. The F8BT layer was spin-cast from a *p*-xylene solution and annealed at 155 °C for 1 h under a N_2 atmosphere. Finally, a 10 nm thick MoO_3 layer and a 60 nm thick Au layer were thermally evaporated at a slow deposition rate of 0.3 Å s^{-1}.

Characterizations. A UV−vis spectrometer (Jasco, V530, Japan) was utilized to measure the optical transmittance of reduced graphene films. The surface roughness and thickness of reduced graphene films were measured by AFM (SPI3800N/SPA400, Seiko Instruments, Inc.). The sheet resistance of reduced graphene was measured by a four-wire sensing system (Keithley 2635 system), and the Hall measurement was performed by a Hall effect measurement system (hms-3000, Ecopia, Korea). XPS measurements were carried out with a Sigma Probe with a microfocused monochromatic X-ray source (Thermo VG Scientific, Inc.). The workfunction of reduced graphene was obtained from ultraviolet photoelectron spectroscopy (AXIS-NOVA, Kratos, Inc.). The current density and luminance *vs* applied voltage characteristics were measured using a Keithley 2400 source measurement unit and a Konica Minolta spectroradiometer (CS-2000).

Acknowledgment. We thank Prof. J.-S. Kim (KAIST WCU Flexible Signage Program) for providing us with F8BT polymer and Dr. J.-H. Park (LG Display) and Prof. S. Park (Inha Univ.) for helpful discussions. This work was financially supported by the National Research Laboratory Program (R0A-2008-000-20057-0), WCU (R32-2008-000-10051-0, R31-2008-000-10071-0) program funded by the Ministry of Education, Science and Technology (MEST) of the Republic of Korea, the Converging Research Center Program through the Ministry of Education, Science and Technology (2011K000642) and LG Display (Material R&D Team).

Supporting Information Available: AFM, SEM, XPS, UPS, Hall measurements, and sheet resistance results are available free of charge *via* the Internet at http://pubs.acs.org.

REFERENCES AND NOTES

1. Novoselov, K. S.; Geim, A. K.; Morozov, S. V.; Jiang, D.; Zhang, Y.; Dubonos, S. V.; Grigorieva, I. V.; Firsov, A. A. Electric Field Effect in Atomically Thin Carbon Films. *Science* **2004**, *306*, 666–669.
2. Geim, A. K. Graphene: Status and Prospects. *Science* **2009**, *324*, 1530–1534.
3. Balandin, A. A.; Ghosh, S.; Bao, W.; Calizo, I.; Teweldebrhan, D.; Miao, F.; Lau, C. N. Superior Thermal Conductivity of Single-Layer Graphene. *Nano Lett.* **2008**, *8*, 902–907.
4. Eda, G.; Fanchini, G.; Chhowalla, M. Large-Area Ultrathin Films of Reduced Graphene Oxide as a Transparent and Flexible Electronic Material. *Nat. Nanotechnol.* **2008**, *3*, 270–274.
5. Kim, K. S.; Zhao, Y.; Jang, H.; Lee, S. Y.; Kim, J. M.; Kim, K. S.; Ahn, J.-H.; Kim, P.; Choi, J.-Y.; Hong, B. H.; *et al*. Large-Scale Pattern Growth of Graphene Films for Stretchable Transparent Electrodes. *Nature* **2009**, *457*, 706–710.
6. Park, S.; Ruoff, R. S. Chemical methods for The Production of Graphene. *Nat. Nanotechnol.* **2009**, *4*, 217–224.
7. Li, X.; Wang, X.; Zhang, L.; Lee, S.; Dai, H. Chemically Derived, Ultrasmooth Graphene Nanoribbon Semiconductors. *Science* **2008**, *319*, 1229–1232.
8. Tung, V. C.; Allen, M. J.; Yang, Y.; Kaner, R. B. High-Throughput Solution Processing of Large-Scale Graphene. *Nat. Nanotechnol.* **2009**, *4*, 25–29.
9. Chae, H. K.; Siberío-Pérez, D. Y.; Kim, J.; Go, Y.; Eddaaoudi, M.; Matzger, A. J.; O'Keeffe, M.; Yaghi, O. M. A Route to High Surface Area, Porosity and Inclusion of Large Molecules in Crystals. *Nature* **2004**, *427*, 523–527.
10. Geim, A. K.; Novoselov, K. S. The Rise of Graphene. *Nat. Mater.* **2007**, *6*, 183–191.
11. Blake, P.; Brimicombe, P. D.; Nair, R. R.; Booth, T. J.; Jiang, D.; Schedin, F.; Ponomarenko, L. A.; Morozov, S. V.; Gleeson, H. F.; Hill, E. W.; Geim, A. K.; Novoselov, K. S.; *et al.* Graphene-Based Liquid Crystal Device. *Nano Lett.* **2008**, *8*, 1704–1708.
12. Han, T. H.; Lee, W. J.; Lee, D. H.; Kim, J. E.; Choi, E.-Y.; Kim, S. O. Peptide/Graphene Hybrid Assembly into Core/Shell Nanowires. *Adv. Mater.* **2010**, *22*, 2060–2064.
13. Kim, B. H.; Kim, J. Y.; Jeong, S.-J.; Hwang, J. O.; Lee, D. H.; Shin, D. O.; Choi, S. Y.; Kim, S. O. Surface Energy Modification by Spin Cast, Large Area Graphene Film for Block Copolymer Lithography. *ACS Nano* **2010**, *4*, 5464–5470.
14. Kim, J. E.; Han, T. H.; Lee, S. H.; Kim, J. Y.; Ahn, C. W.; Yun, J. M.; Kim, S. O. Graphene Oxide Liquid Crystals. *Angew. Chem., Int. Ed.* **2011**, *50*, 3043–3047.
15. Jeong, H. Y.; Kim, J. Y.; Kim, J. W.; Hwang, J. O.; Kim, J. E.; Lee, J. Y.; Yoon, T. H.; Cho, B. J.; Kim, S. O.; Ruoff, R. S.; Choi, S. Y.; *et al.* Graphene Oxide Films for Flexible Nonvolatile Memory Application. *Nano Lett.* **2010**, *10*, 4381–4386.
16. Lee, S. H.; Kim, H. W.; Hwang, J. O.; Lee, W. J.; Kwon, J.; Bielawski, C. W.; Ruoff, R. S.; Kim, S. O. Three-Dimensional Self-Assembly of Graphene Oxide Platelets into Mechanically Flexible Macroporous Carbon Films. *Angew. Chem., Int. Ed.* **2010**, *49*, 10084–10088.
17. Wang, X.; Zhi, L.; Müllen, K. Transparent, Conductive Graphene Electrodes for Dye-Sensitized Solar Cells. *Nano Lett.* **2008**, *8*, 323–327.
18. Hwang, J. O.; Lee, D. H.; Kim, J. Y.; Han, T. H.; Kim, B. H.; Park, M.; No, K.; Kim, S. O. Vertical ZnO Nanowires/Graphene Hybrids for Transparent and Flexible Field Emission. *J. Mater. Chem.* **2011**, *21*, 3432–3437.
19. Rani, A.; Nam, S.; Oh, K. A.; Park, M. Electrical Conductivity of Chemically Reduced Graphene Powders under Compression. *Carbon Lett.* **2010**, *11*, 90–95.
20. Liu, W.; Do, I.; Fukushima, H.; Drzal, L. T. Influence of Processing on Morphology, Electrical Conductivity and Flexural Properties of Exfoliated Graphite Nanoplatelets−Polyamide Nanocomposites. *Carbon Lett.* **2010**, *11*, 279–284.

21. Kuzmenko, A. B.; van Heumen, E.; Carbone, F.; van der Marel, D. Universal Optical Conductance of Graphite. *Phys. Rev. Lett.* **2008**, *100*, 117401–1.
22. Li, X.; Cai, W.; An, J.; Kim, S.; Nah, J.; Yang, D.; Piner, R.; Velamakanni, A.; Jung, I.; Tutuc, E.; Banerjee, S. K.; Colombo, L.; Ruoff, R. S.; *et al.* Large-Area Synthesis of High-Quality and Uniform Graphene Films on Copper Foils. *Science* **2009**, *324*, 1312–1314.
23. Avsar, A.; Yang, T. −Y.; Bae, S.; Balakrishnan, J.; Volmer, F.; Jaiswal, M.; Yi, Z.; Ali, S. R.; Güntherodt, G.; Hong, B. H.; Beschoten, B.; Özyilmaz, B.; *et al.* Toward Wafer Scale Fabrication of Graphene Based Spin Valve Devices. *Nano Lett.* **2011**, *11*, 2363–2369.
24. Wang, C. Y.; Mylvaganam, K.; Zhang, L. C. Wrinkling of Monolayer Graphene: A Study by Molecular Dynamics and Continuum Plate Theory. *Phys. Rev. B* **2009**, *80*, 155445–1.
25. Stankovich, S.; Dikin, D. A.; Piner, R. D.; Kohlhaas, K. A.; Kleinhammes, A.; Jia, Y.; Wu, Y.; Nguyen, S. T.; Ruoff, R. S. Synthesis of Graphene-Based Nanosheets *via* Chemical Reduction of Exfoliated Graphite Oxide. *Carbon* **2007**, *45*, 1558–1565.
26. Park, S.; An, J.; Jung, I.; Piner, R. D.; An, S. J.; Li, X.; Velamakanni, A.; Ruoff, R. S. Colloidal Suspensions of Highly Reduced Graphene Oxide in a Wide Variety of Organic Solvents. *Nano Lett.* **2009**, *9*, 1593–1597.
27. Gomez-Navarro, C.; Weitz, R. T.; Bittner, A. M.; Scolari, M.; Mews, A.; Burghard, M.; Kern, K. Electronic Transport Properties of Individual Chemically Reduced Graphene Oxide Sheets. *Nano Lett.* **2007**, *7*, 3499–3503.
28. Li, D.; Muller, M. B.; Gilje, S.; Kaner, R. B.; Wallace, G. G. Processable Aqueous Dispersions of Graphene Nanosheets. *Nat. Nanotechnol.* **2008**, *3*, 101–105.
29. Gao, W.; Alemany, L. B.; Ci, L.; Ajayan, P. M. New Insights into the Structure and Reduction of Graphite Oxide. *Nat. Chem.* **2009**, *1*, 403–408.
30. Stankovich, S.; Piner, R. D.; Chen, X.; Wu, N.; Nguyen, S. T.; Ruoff., R. S. Stable Aqueous Dispersions of Graphitic Nanoplatelets *via* the Reduction of Exfoliated Graphite Oxide in the Presence of Poly(sodium 4-styrenesulfonate). *J. Mater. Chem.* **2006**, *16*, 155–158.
31. Becerril, H. A.; Mao, J.; Liu, Z.; Stoltenberg, R. M.; Bao, Z.; Chen, Y. Evaluation of Solution-Processed Reduced Graphene Oxide Films as Transparent Conductors. *ACS Nano* **2008**, *2*, 463–470.
32. Hernandez, Y.; Nicolosi, V.; Lotya, M.; Blighe, F. M.; Sun, Z.; De, S.; McGovern, I. T.; Holland, B.; Byrne, M.; Gun'Ko, Y. K.; *et al.* High-Yield Production of Graphene by Liquid-Phase Exfoliation of Graphite. *Nat. Nanotechnol.* **2008**, *3*, 563–568.
33. Englert, J. M.; Dotzer, C.; Yang, G.; Schmid, M.; Papp, C.; Gottfried, J. M.; Steinrück, H.-P.; Spiecker, E.; Hauke, F.; Hirsch, A.; et al. Covalent Bulk Functionalization of Graphene. *Nat. Chem.* **2011**, *3*, 279–286.
34. Park, S.; Hu, Y.; Hwang, J. O.; Lee, E. -S.; Casabianca, L. B.; Cai, W.; Potts, J. R.; Ha, H.-W.; Chen, S.; Oh, J.; Kim, S. O.; Kim, Y.-H.; Ishii, Y.; Ruoff, R. S. Chemical Structures of Hydrazine-Treated Graphene Oxide and Generation of Aromatic Nitrogen Doping. *Nat. Commun.* **2011** (accepted, NCOMMS-11-01728A).
35. Matyba, P.; Yamaguchi, H.; Eda, G.; Chhowalla, M.; Edman, L.; Robinson, N. D. Graphene and Mobile Ions: The Key to All-Plastic, Solution-Processed Light Emitting Devices. *ACS Nano* **2010**, *4*, 637–642.
36. Wu, J.; Agrawal, M.; Becerril, H. A.; Bao, Z.; Liu, Z.; Chen, Y.; Peumans, P. Organic Light-Emitting Diodes on Solution-Processed Graphene Transparent Electrodes. *ACS Nano* **2010**, *4*, 43–48.
37. Zheng, Q; Ip, W. H.; Lin, X.; Yousefi, N.; Yeung, K. K.; Li, Z.; Kim, J. K. Transparent Conductive Films Consisting of Ultralarge Graphene Sheets Produced by Langmuir−Blodgett Assembly. *ACS Nano* **2011**, *5*, 6039–6051.
38. Li, X.; Wang, H.; Robinson, J. T.; Sanchez, H.; Diankov, G.; Dai, H. Simultaneous Nitrogen Doping and Reduction of Graphene Oxide. *J. Am. Chem. Soc.* **2009**, *131*, 15939–15944.
39. De, S.; Coleman, J. N. Are There Fundamental Limitations on the Sheet Resistance and Transmittance of Thin Graphene Films? *ACS Nano* **2010**, *4*, 2713–2720.
40. Lee, D. H.; Lee, W. J.; Lee, W. J.; Kim, S. O.; Kim, Y. -H. Theory, Synthesis, and Oxygen Reduction Catalysis of Fe-Porphyrin-Like Carbon Nanotube. *Phys. Rev. Lett.* **2011**, *106*, 175502–1.
41. Sessolo, M.; Bolink, H. J. Hybrid Organic-Inorganic Light-Emitting Diodes. *Adv. Mater.* **2011**, *23*, 1829–1845.
42. Friend, R. H.; Gymer, R. W.; Holmes, A. B.; Burroughes, J. H.; Marks, R. N.; Taliani, C.; Bradley, D. D. C.; Dos Santos, D. A.; Brédas, J. L.; Lögdlund, M.; Salaneck, W. R.; *et al.* Electroluminescence in Conjugated Polymers. *Nature* **1999**, *397*, 121–128.
43. Park, J. S.; Lee, B. R.; Lee, J. M.; Kim, J. S.; Kim, S. O.; Song, M. H. Efficient Hybrid Organic-Inorganic Light Emitting Diodes with Self-Assembled Dipole Molecule Deposited Metal Oxides. *Appl. Phys. Lett.* **2010**, *96*, 243306–1.
44. Morii, K.; Kawase, T.; Inoue, S. High Efficiency and Stability in Air of The Encapsulation-Free Hybrid Organic-Inorganic Light Emitting Diodes. *Appl. Phys. Lett.* **2008**, *92*, 213304–1.
45. Kabra, D.; Song, M. H.; Wenger, B.; Friend, R. H.; Snaith, H. J. Efficient Single-Layer Polymer Light-Emitting Diodes. *Adv. Mater.* **2010**, *22*, 3194–3198.
46. Bolink, H. J.; Coronado, E.; Orozco, J.; Sessolo, M. Efficient Polymer Light-Emitting Diode Using Air-Stable Metal Oxides as Electrodes. *Adv. Mater.* **2009**, *21*, 79–82.
47. Tokmoldin, N.; Griffiths, N.; Bradley, D. D. C.; Haque, S. A. A Hybrid Inorganic-Organic Semiconductor Light-Emitting diode Using ZrO_2 as an Electron-Injection Layer. *Adv. Mater.* **2009**, 3475–3478.
48. Nakayama, Y.; Morri, K.; Suzuki, Y.; Machida, H.; Kera, S.; Ueno, N.; Kitagawa, H.; Noguchi, Y.; Ishii, H. Origins of Improved Hole-Injection Efficiency by the Deposition of MoO_3 on the Polymeric Semiconductor Poly(dioctylfluorene-*alt*-benzothiadiazole). *Adv. Funct. Mater.* **2009**, *19*, 3746–3752.
49. Song, M. H.; Kabra, D.; Wenger, B.; Friend, R. H.; Snaith, H. J. Optically-Pumped Lasing in Hybrid Organic-Inorganic Light-Emitting Diodes. *Adv. Funct. Mater.* **2009**, *19*, 2130–2136.
50. Matyba, P.; Yamaguchi, H.; Eda, G.; Chhowalla, M.; Edman, L.; Robinson, N. D. Graphene and Mobile Ions: The Key to All-Plastic, Solution-Processed Light-Emitting Devices. *ACS Nano* **2010**, *4*, 637–642.
51. Lee, T.-W.; Hwang, J.; Min, S.-Y. Highly Efficient Hybrid Inorganic-Organic Light-Emitting Diodes by using Air-Stable Metal Oxides and a Thick Emitting Layer. *ChemSusChem* **2010**, *3*, 1021–1023.
52. Gong, X.; Lim, S.-H.; Ostrowski, J. C.; Moses, D.; Bardeen, C. J.; Bazan, G. C. Phosphorescence from Iridium Complexes Doped into Polymer Blends. *J. Appl. Phys.* **2004**, *95*, 948–953.
53. Cao, Y.; Yu, G.; Parker, I. D.; Heeger, A. J. Ultrathin Layer Alkaline Earth Metals as Stable Electron-Injecting Electrodes for Polymer Light Emitting Diodes. *J. Appl. Phys.* **2000**, *88*, 3618–3623.
54. Krebs, F. C. Encapsulation of Polymer Photovoltaic Prototypes. *Sol. Energy Mater. Sol. Cells* **2006**, *90*, 3633–3643.
55. Weaver, M. S.; Michalski, L. A.; Rajan, K.; Rothman, M. A.; Silvernail, J. A. Organic Light-Emitting Devices with Extended Operating Lifetimes on Plastic Substrates. *Appl. Phys. Lett.* **2002**, *81*, 2929–2931.
56. Lee, D. H.; Lee, J. A.; Lee, W. J.; Kim, S. O. Flexible Field Emission of Nitrogen-Doped Carbon Nanotubes/Reduced Graphene Hybrid Films. *Small* **2011**, *7*, 95–100.
57. Luo, Z.; Lim, S.; Tian, Z.; Shang, J.; Lai, L.; MacDonald, B.; Fu, C.; Shen, Z.; Yu, T.; Lin, J.; *et al.* Pyridinic N Doped Graphene: Synthesis, Electronic Structure, and Electrocatalytic Property. *J. Mater. Chem.* **2011**, *21*, 8038–8044.
58. Soin, N.; Roy, S. S.; Roy, S.; Hazra, K. S.; Misra, D. S.; Lim, T. H.; Hetherington, C. J.; McLaughlin, J. A. Enhanced and Stable Field Emission from In-Situ Nitrogen-Doped Few-Layered Graphene Nanoflakes. *J. Phys. Chem. C* **2011**, *115*, 5366–5372.
59. Yu, Y.-J.; Zhao, Y.; Ryu, S.; Brus, L. E.; Kim, K. S.; Kim, P. Tuning the Graphene Work Function by Electric Field Effect. *Nano Lett.* **2009**, *9*, 3430–3434.
60. Hibini, H.; Kageshima, H.; Kotsugi, M.; Maeda, F.; Guo, F.-Z.; Watanabe, Y. Dependence of Electric Properties of

Epitaxial Few-Layer Graphene on the Number of Layers Investigated by Photoelectron Emission Microscopy. *Phys. Rev. B* **2009**, *79*, 125437–1.
61. Wei, D.; Liu, Y.; Wang, Y.; Zhang, H.; Huang, L.; Yu, G. Synthesis of N-Doped Graphene by Chemical Vapor Deposition and Its Electrical Properties. *Nano Lett.* **2009**, *9*, 1752–1758.
62. Wang, X.; Liu, Y.; Zhu, D.; Zhang, L.; Ma, H.; Yao, N.; Zhang, B. Controllable Growth, Structure, and Low Field Emission of Well-Aligned CN_x Nanotubes. *J. Phys. Chem. B* **2002**, *106*, 2186–2190.
63. Baek, W.-H.; Choi, M.; Yoon, T.-S.; Lee, H. H.; Kim, Y.-S. Use of Fluorine-Doped Tin Oxide Instead of Indium Tin Oxide in Highly Efficient Air-Fabricated Inverted Polymer Solar Cells. *Appl. Phys. Lett.* **2010**, *96*, 133506–1.
64. Sugiyama, K.; Ishii, H.; Ouchi, Y. Dependence of Indium-Tin-Oxide Work Function on Surface Cleaning Method as Studied by Ultraviolet and X-Ray Photoemission Spectroscopies. *J. Appl. Phys.* **2000**, *87*, 295–298.
65. Lee, D. H.; Lee, W. J.; Kim, S. O. Highly Efficient Vertical Growth of Wall-Number-Selected, N-Doped Carbon Nanotube Arrays. *Nano Lett.* **2009**, *9*, 1427–1432.